Publishing Excellence
Inspiring Progress
ARISTON PUBLICATIONS

Energy & Environment Advances

ISSN: xxxx-xxxx https://aristonpubs.com/energy-environment-advances https://doi.org/10.69626/eea.2024.0004

RESEARCH ARTICLE

Significant Enhancement in Surface Passivation Property of Micro–Textured Silicon Surface with Thin Hydrogenated Intrinsic Amorphous Layer

Diksha [1,2], Shrestha Bhattacharya [3], Riya Bansal [1,2], Meenakshi [1,2], Ashutosh Pandey [3], Prathap Pathi [1,2], Vamsi K. Komarala [3], Sanjay K. Srivastava [1,2,*]

ABSTRACT: In the present study, one step low-cost alkaline potassium hydroxide (aqueous solution) method was implemented on Czochralski silicon and Float zone silicon wafers for micro-texturing under identical parameters that improve light harvesting property of the wafers. At the rear interface of micro-textured Czochralski and Float zone silicon, a few nm thin layer of hydrogenated intrinsic amorphous silicon and n-type nano crystalline silicon was deposited, which not only addressed the parasitic loses at rear interfaces but also provides excellent passivation via back surface field to the micro-textured silicon surfaces. The minority carrier life time measurement was done on symmetric structure (i-a-Si:H/µT-n-Si/i-a-Si:H). The minority carrier lifetime is found 2.31 µs and 677.79 µs for the unpassivated and hydrogenated intrinsic amorphous silicon passivated micro-textured silicon Czochralski surfaces. Similarly, the measured lifetime of the micro-textured Float zone for unpassivated and passivated silicon surfaces are found 2.77 µs and 1788.30 µs. The high implied open circuit voltage of the micro-textured silicon wafers after deposition of hydrogenated intrinsic amorphous silicon (for passivated Czochralski and Float zone silicon are 708 mV and 714 mV respectively) indicates improvement in the collection property of electrons at the cathodic interface. The reflectance data, measured on symmetric structure, before and after hydrogenated intrinsic amorphous silicon layer deposition confirms that the incorporation of passivation layer does not affect light harvesting property of the micro-textured silicon wafers. Thus, stack of hydrogenated intrinsic amorphous/n-nano-crystalline silicon thin layers could be an effective interface passivation layer for futuristic high-performance hetero-junction solar cells (HJSCs) i.e., HIT, hybrid solar cells under optimize parameters for full potential.

Keywords: Minority Carrier Lifetime (MCLT), Passivation, Back Surface Field (BSF), Interface Defect Density, hydrogenated intrinsic amorphous silicon (i-a-Si:H) layer, n-type nano-crystalline silicon (n-nc-Si:H).

Received: 13 January 2024; Revised: 15 February 2024; Accepted: 16 February 2024; Published Online: 01 March 2024

1. INTRODUCTION

The consumption of fossil fuels has pushed our environment and humanity towards natural chaos with increasing global warming [1]. This rise in quantity of harmful gases i.e. carbon dioxide (CO_2) in atmosphere brings hazardous condition for our planet in near future. It becomes crucial need to approach non-conventional energy sources to fulfill our day-to-day energy requirements. Solar energy, wind energy, biomass energy, geothermal energy, hydro-power energy are some of non-conventional energy sources. But solar energy has been regarded as an ideal alternative energy source; this energy source has received great attention in recent decades due to its capability to meet global energy requirements [2]. The crystalline silicon (c-Si) solar cells are the dominating ones in today's commercial photovoltaics (PV) market with a current share of ~ 95 % for solar cells manufacturing

[1] Photovoltaic Metrology Section, Adavanced Materials and Device Metrology Division, CSIR-National Physical Laboratory, New Delhi 110012, India.
[2] Academy of Scientific and Innovative Research (AcSIR), Ghaziabad, Uttar Pradesh, 201002, India.
[3] Solar Photovoltaics Laboratory, Department of Energy Science and Engineering, Indian Institute of Technology Delhi, New Delhi 110016, India.

* Author to whom correspondence should be addressed: srivassk@nplindia.org (S. K. Srivastava)

process due to properties of Si material itself i.e. 2nd most abundance on earth, high stability and durability, non-toxic, tunable optoelectronic properties, mature manufacturing processes, etc [3].

The basic working mechanism of a PV solar cells relates to the generation of photo carriers, and the effective collection of these photo-generated photo carriers to external electrodes. Both these process are highly effected by reflection and parasitic recombination losses during generation as-well transportation of photo-carriers, which then responsible for deteriorate performance of solar cells if not addressed properly [4]. The as-cut Si surface have reflectivity > 35% in broad spectral range 400 nm-1100 nm, so for advancement of Si solar cells, surface reflection related optical as well as passivation related electrical losses are required to be minimized. In order to achieve highly optically active surfaces, which not only reduces reflection losses but also enhance the light absorption various surface modification schemes like micro-texturing, nano-texturing, hierarchical schemes of light trapping were used. The nano structured Si can harvest light up to 98% of incident light but simultaneously enhanced junction area of Si, wherein surface recombination of the photo-generated carriers increases due to high interfacial as well as surface defect densities [5-7]. The nano structured morphology of Si also enhance the hydrophobic nature of Si surface which then create problem in making junction [8]. Hierarchical scheme of light trapping can reduce reflection even < 1% under highly optimized specific wavelengths (narrow range) and light angles but for broad wavelength range it can reduce refection < 5% [9, 10]. Creating hierarchical structured Si surface involves complex fabrication process, complexity of junction formation, enhance contact resistance (which can enhance parasitic resistance recombination losses), high cost production along with time consuming process [11]. The most effective, industry approved and scientifically accepted approach for cost efficient, thermally compatible, and easy to process solar cell fabrication and single-step is alkaline micro-texturing. This method reduces surface reflection losses by surface conditioning of Si wafer and simultaneously addressing the challenges of hydrophobicity in Si solar cell [12-14]. Srivastava et al. 2021 delve into the specific benefits of KOH texturing on low-cost, solar-grade silicon wafers as a method to enhance the efficiency of PEDOT:PSS/Silicon hybrid solar cells.[8]

After have control over surface reflection losses next challenge is to passivate the surface to minimize contact/parasitic resistance losses during the transportation of the generated photo carriers to the external storage device, which is also an important step in enhancing the solar cell efficiency. The bulk MCLT is an important parameter that limits the solar cell efficiency and can be used to monitor the material quality. There are various techniques available for determining MCLT of Si wafer like microwave reflectance photoconductive decay method, electrochemical impedance spectroscopy, transient and QSS (quasi-steady state) photo conductance method [15-17]. MCLT measurement is a direct way to observe the passivation nature of particular material/film because it is directly related to surface defects density, inter-facial defect density, surface recombination velocity (SRV). Therefore, reduction of such recombination is a key step in obtaining highly passivated surface. An effective surface passivation involve two complementary mechanisms. First, a decrease in the number of dangling bonds by saturating the orbitals of Si atom on semiconductor Si surface. Secondly, limiting the number of carriers available for recombination using an induced electric field and is achieved by having a fix charge in the dielectric/amorphous/nano-crystalline film either by built-in charges during deposition process or by controllably deposited in a separate step [18]. As an industrial point of view, dielectric layers such as SiO_x, Si_xN_y, $Al_2O_,$ are generally used for Si surface passivation but the growth of such layer on Si surface requires high thermal process wherein lifetime degradation associated with hight thermal budget cannot be ruled out [19]. Various other passivation layers like MoO3, ZnO, AZO, HfO, TiO_2, SnO_2, CdS, In_3Se_4, $BaSnO_3$ even stack of different layer like TiO_2/graphene, TiO_2/ZnO, TiO_2/WO_3 are also used as passivation layers. These layers deposited by different techniques i.e. atomic layer deposition (ALD) system, plasma enhanced chemical vapour deposition (PECVD), metal-organic chemical vapour deposition (MOCVD), pulse layer deposition (PLD), sputtering, sol-gel method, etc [20-23]. The i-a-Si:H layer deposited at low temperature provides prime-quality surface passivation by saturating the dangling bonds on the H-terminated c-Si surface and it also work as a tunnel layer under optimized few nm thickness [24-26]. The n-nc-Si:H layer provides best interfacial effective passivation via BSF compared to doped a-Si:H layer due to better optoelectronics properties, thermal stability and high optical bandgap [27]. The stack of i-a-Si:H and n-nc-Si:H layers provides an effective surface passivation, which is beneficial in manufacturing Si solar cells of enhanced efficiency.

Hence, the motivation behind the present work is to enhance optical property of Si surfaces and improving the back surface passivation of Si by most effective passivation layers. In this present work, we report a systematic surface conditioning scheme and surface passivation study made on phosphorous doped CZ-Si as well as on FZ-Si. Also investigate how the two different quality of Si samples get affected by simple low-cost, single-step anisotropic etching in aqueous alkaline KOH solution. A detailed study is done on reflectance, lifetime and morphology of Si surfaces, which conclude the better passivation characteristics of i-a-Si:H layer on both type of Si materials.

2. EXPERIMENTAL DETAILS

2.1. Surface modification of wafers and i-a-Si:H/n-nc-Si:H layers deposition

As-cut commercial available, solar grade phosphorous doped (n-type), 1-3 Ω-cm resistivity, 200 ±20 µm thick CZ-Si (100)

and 1-5 Ω-cm resistivity, 260-300 µm thick, phosphorous doped FZ-Si (100) wafers are used as the starting material. Samples of dimension 40x40 mm^2 from CZ-Si, 35x35 mm^2 from FZ-Si are first diced from starting as-cut Si wafers so that samples have identical material specification i.e. doping concentration, sheet resistance, conductivity etc. Both type of samples were treated individually. In the very first step, the samples were cleaned sequentially in de-ionized (DI) water, acetone and IPA to remove organic residues and other mechanical impurities (sand, crystalline salt, dust particles etc.) from Si surface by ultrasonication for 10 min each. Aqueous alkaline solution was prepared for anisotropic etching of Si wafer consist of DI, 2 % (wt%) KOH and 20% (v/v) IPA. Then, the Si wafers were immersed in aqueous alkaline solution maintained at constant temperature 75 ± 5˚C for 60 min. CZ-Si as well FZ-Si were etched in separate batches. The i-a-Si:H layer deposited by multi-chambered RF plasma enhanced chemical vapor deposition (PECVD) system with 13.56 MHz frequency generator. After texturing, wafers were given RCA 1 and RCA2 cleaning, followed by HF dip in (~ 1% HF) just before sample loaded in chamber for deposition so that extra native Si oxides, organic/metallic impurities get removed from Si wafers. The i-a-Si:H layer of ~ 8 nm deposited in SiH_4/H_2 plasma with dilution ratio of 1:1, 40 sscm each (SiH_4 as well H_2) at a temperature of 215˚C and 0.37 torr pressure. The n-nc-Si:H layer (18 nm) deposited by same multi-chambered RF-PECVD system, but with increased frequency (27.12 MHz) in a separate chamber at different parameters. The silane (SiH_4) to hydrogen (H_2) gas ratio was 1:200 (i.e. 2 sccm SiH_4 and 400 sccm H_2), 200˚C deposition temperature and 1 torr pressure along with supply of phosphine (PH_3) gas (4 % in SiH_4). Power density was same during deposition of both layers i.e. 122 mw/cm^2 [27].

2.2. Characterization

The surface morphology of µT CZ-Si and FZ-Si (bare and with stack of passivation layers) is investigated by field emission scanning electron microscopy (FE-SEM, Model: TESCAN Magna GMH). For the FESEM micrographs (lateral as well as cross-sectional), the stack of i-a-Si:H/n-nc-Si layers was deposited on rear side of the µT-Si wafers. Reflectance measurements are the direct consequences of light harvesting property of the modified surfaces. Therefore, reflectance of as-cut, textured Si wafers were performed to investigate photons capturing ability of Si surface after pyramidal growth on CZ and FZ Si wafers. Also, to see effect of i-a-Si:H layer on optical properties of textured samples, reflectance measurement of µT samples with deposited layer was recorded. So, the total reflectance measurement of all samples CZ as well as FZ (as-cut, µT and µT-i-a-Si:H/n-nc-Si:H) was done by using UV-VIS-NIR photo spectroscopy (Lambda 1050; PerkinElmer) at a normal incidence angle of ~ 8˚ of light, equipped with an integrating sphere, in abroad spectral range (300 nm-1200 nm).

The minority carrier lifetime is an important parameter to investigate the passivation ability of a particular material. MCLT of as-cut, µT and i-a-Si:H layered samples are recorded by Sinton's instrument (model: WCT-120), that works on quasi-steady state (QSS), transient as well in generalized photoconductive decay mode. For MCLT measurement, the i-a-Si:H layer (~ 8 nm each side) is deposited on both side of textured Si wafers of both types. Here, in the present case, in QSS as well as in transient photoconductive mode measurements were performed depending upon the MCLT range. Finally, the all over optical properties of pyramidal Si surface and also the passivation properties of i-a-Si:H and n-nc-Si:H layer each on CZ as well FZ were studied.

3. RESULTS AND DISCUSSION

3.1. Micro-textured Si surface morphology and optical study

To investigate how the as-cut Si surfaces get modified after treating with KOH aqueous alkaline solution, systematic lateral as well as cross-sectional analysis of FE-SEM micrographs was performed. Figure 1 shows micrographs starting with as-cut Si (Figure 1(a)) wafer that is used as a starting material in this present work. As cut Si wafer contains a large number of micro-cracks, pits, and so-called surface damages/saw damages on the whole surface that can't never be seen by naked eyes. Crystalline Si of either material CZ or FZ when treated with aqueous alkaline solution, micro-pyramidal structures are nucleated due to anisotropic etching of Si surface in different crystallographic orientations (Figure 1(b)-(f)). It can be explained, the ternary liquid etching solution here consist of KOH, IPA and DI-water, in which each have its specific role in anisotropic etching process. KOH as an oxidant, IPA as a complexing agent or reaction modulating agent (plane orientation dependent) and DI-water as a catalyst, interact with Si surface in such a way, results in pyramidal growth over the entire Si surface discussed here via chemical kinetics [13,14]. As the (100) plane of Si atom have two dangling bonds on the surface (Figure 2.). In the very first step after immersing Si (100) in aqueous alkaline solution, the two hydroxyl (OH-) ions from alkaline solution make bond with the two dangling bond of superficial Si and established silicon hydroxide (Si-OH) complex along with injection of two electrons into conduction band (CB) of Si as shown in below equation.

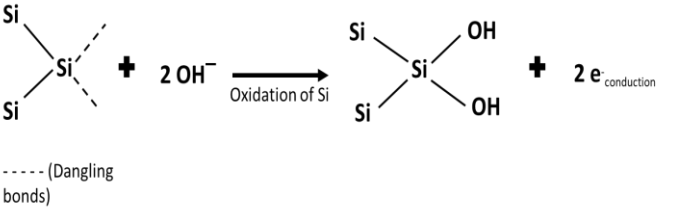

In the next step, these two newly formed Si-OH bond weaken the two backbond of the Si.

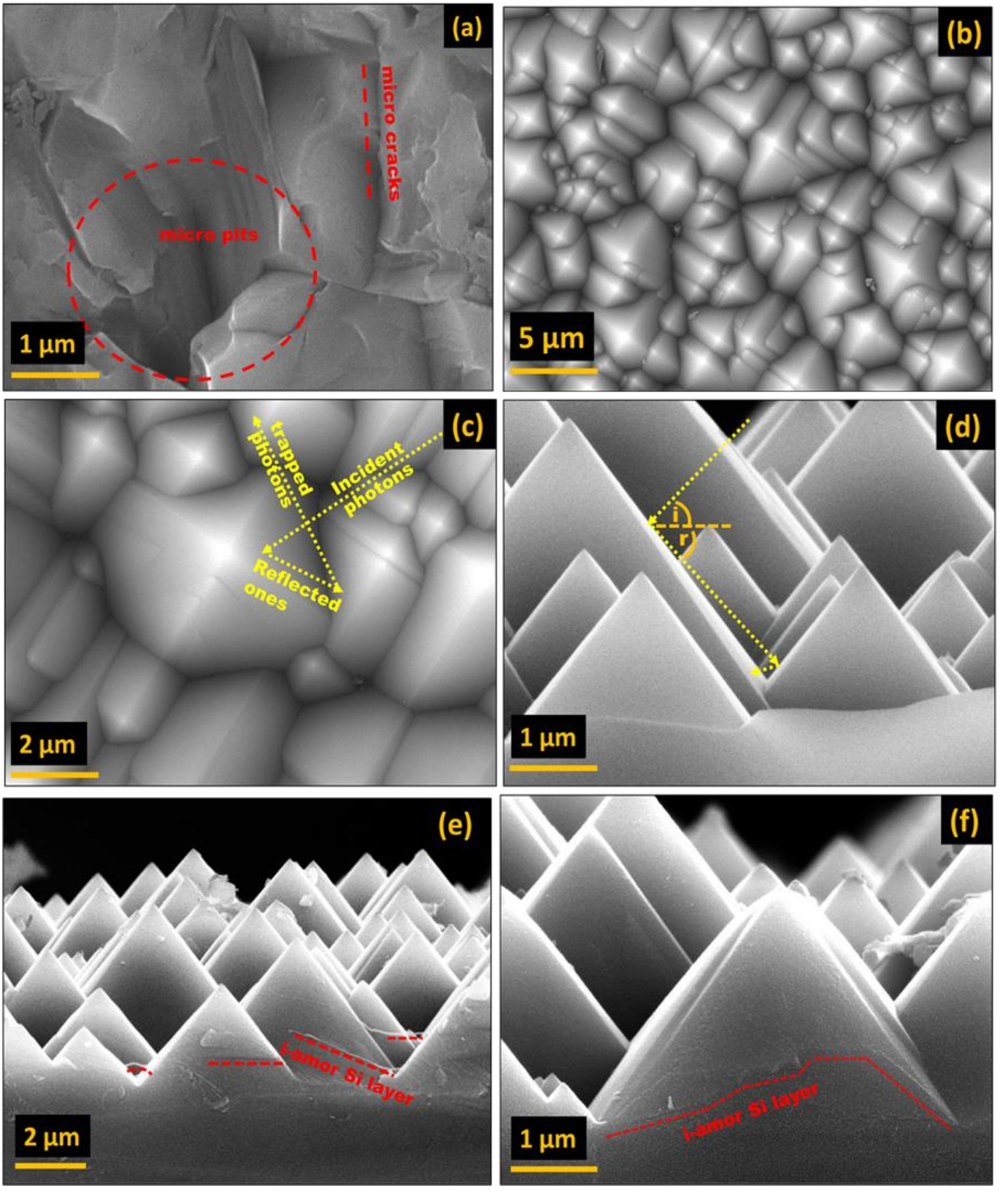

Fig. 1. Representative FESEM micrographs of Si showing surface morphology after surface modification (a) as-cut Si, (b-c) lateral view of textured wafer. (d) cross-sectional view of textured wafer. (e-f) textured cross-sectional view of wafers with i-a-Si:/n-nc-Si:H stack that confirms the conformal deposition of the stack over textured morphology.

To break these weaken backbonds (Figure 2), two electrons from Si-Si backbonds have to be excited to Si CB and once this happen, the Si-Si back bonds break and a positive silicon hydroxide is formed as shown in the below equation:

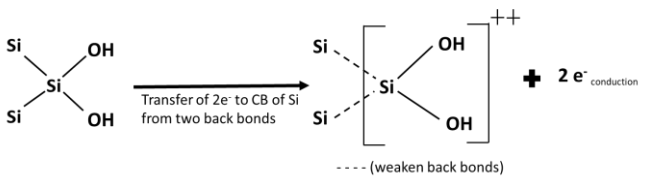

Then, the Si-OH positive complex further react with the other two OH- ions from aq alkaline solution to produce reaction product i.e. monosalicylic acid etc, which then diffused into the solution.

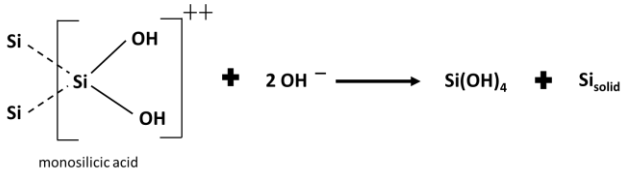

The four electrons, which are in the CB of Si (located near the surface) can be transferred to four water molecules (also located near the surface of Si), which further decompose four water molecules into OH- ions and hydrogen atom. Atomic hydrogen further recombines to produce molecular hydrogen, which may then diffuse into the solution or may get evaporated as hydrogen gas as demonstrated in the below equation:

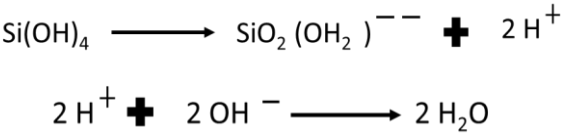

In this mechanism, IPA acts as a mask against chemical reactants (like SiOx) in particular planes, regulates the etching rate for solutions with a constant KOH concentration and constant temperature. It is more absorbed on (111) plane compared to (100) plane (in (111) plane atoms forms a dense triangular lattice, leading to a higher atomic density. Due to this triangular arrangement more atoms of Si are packed in (111) plane and hence more absorption of IPA in this plane) of Si, results that IPA stimulate and responsible for the anisotropic etching (formation of pyramids) of Si surface [28]. This anisotropic etching produce uniform morphological micro-pyramidal features on the entire Si surface basically due to IPA, if etching of wafers without IPA is performed it will etch entire Si surface in all planes uniformly and thus leads to thinning of Si wafer instead of pyramidal etching [29]. The lateral and cross-sectional view of micro-pyramidal surfaces shown in Figure 1. A detailed statistical analysis of the dimension of the micrographs was conducted by employing the imageJ software on several FE-SEM images of respective (CZ and FZ) Si samples.

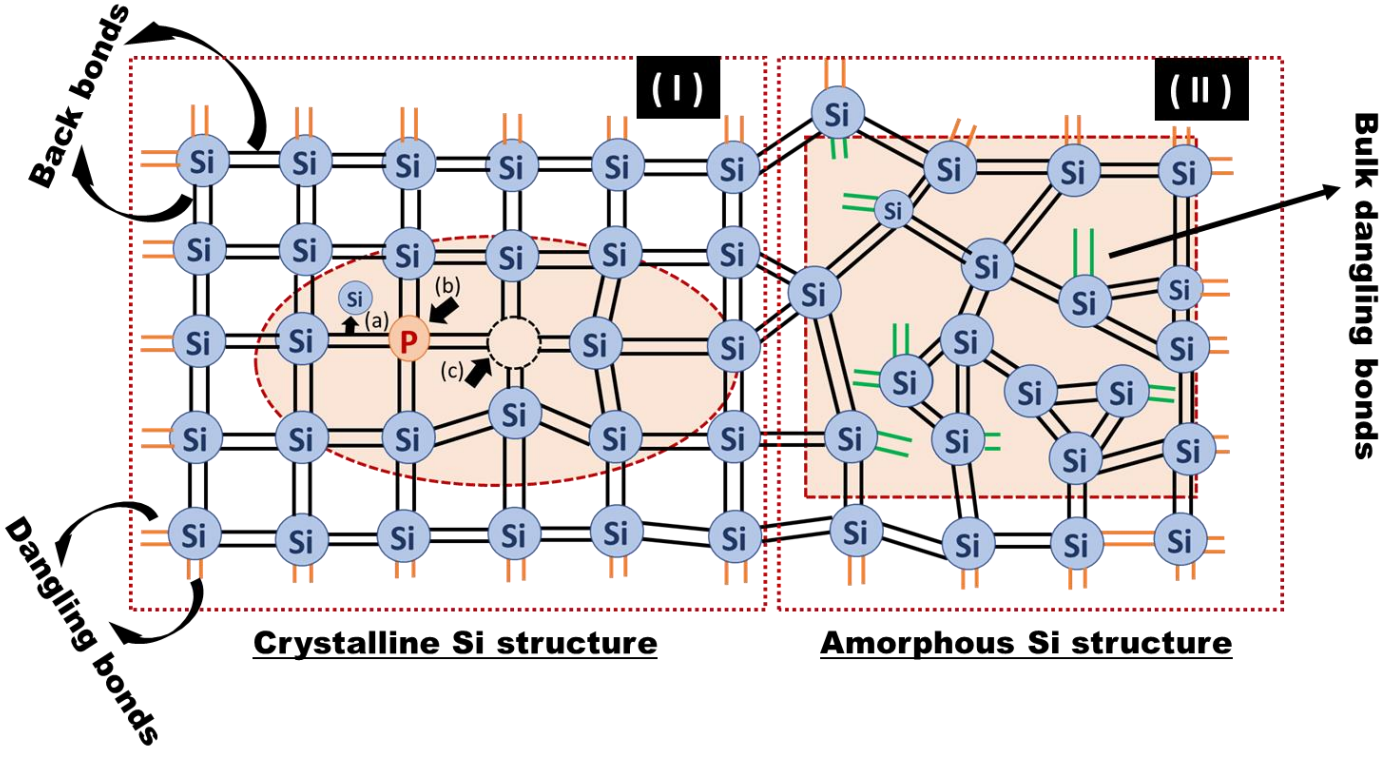

Fig. 2. (I) Crystalline Si showing periodic arrangement of Si atoms along with bulk defects (a) interstitial defects. (b) and (c) vacancy defects, surface defects i.e. dangling bonds, (II) Amorphous Si contains large number of unoccupied interior dangling states.

The dimension of the micro-pyramids for CZ µT-Si vary in the range of ~ 0.5 µm to 5.6 µm (on an average ~ 2.41 µm) and ~ 0.4 µm to 8.9 µm (average over ~ 3.44 µm) for FZ µT-Si wafer. The surface morphology of different Si samples was also investigated after deposition of i-a-Si:H/n-nc-Si:H layers at rear side of textured wafer as shown in Figure 1(e-f), indicates almost uniform coverage of entire pyramids including hills as well as valley. The diffused reflectance measurement is done before and after layers depositions via UV-VIS-NIR photo spectroscopy in broad spectral range (400 nm to 1200 nm). SWR is used for evaluating the optical properties of Si surface, it is defined as the ratio of reflected photons to the total number of incident photons, i.e., the normalization of reflectance spectra with the terrestrial air mass 1.5 global (AM 1.5G) as given below [30]:

$$\text{SWR} = \frac{\int R(\lambda) N_{ph}(\lambda) d\lambda}{\int N_{ph}(\lambda) d\lambda} \quad (1)$$

Where, N_{ph} is the number of photons per unit area per unit wavelength. Using equation (1), the SWR is calculated for the as-cut, µT as well as i-a-Si:H layered CZ and FZ surfaces which is shown in Figure 3.

The calculated SWR for CZ-Si material of as-cut and after micro-pyramidal morphology is 31.23 % and 12.93 % respectively. Similarly, SWR for FZ Si material is 26.72 % and 13.90 % before and after micro-texturing, which indicated that in both material of Si reflectivity get reduced approximately ~2.4 folds and ~ 2 folds respectively; followed by increased path length of incident light due to multiple reflection (obeying the basic laws of reflection shown in Figure 1 (d)) from different facets of upright pyramids (Figure 1(c)). The reflected light from pyramid surfaces produce destructive interference due to enhanced path length, which results in increased absorption capability of modified textured Si surfaces. Also, noted that, the calculated SWR for CZ after i-a-Si layer is 13.60 % (~1 folds compared to bare CZ textured surface) and 14.07 % (~ 1folds than bare FZ textured surface) for FZ after i-a-Si:H layer deposition, which clearly indicate that optical properties of micro-pyramidal Si surfaces get not much affected by insertion of intrinsic amorphous layers. Thus, if the i-a-Si:H layer (with optimize parameters) used on front side (along with rear) of textured surface also, then it does not have deteriorating effect on optical properties of Si surfaces and also enhance inter-facial properties during solar cell fabrication.

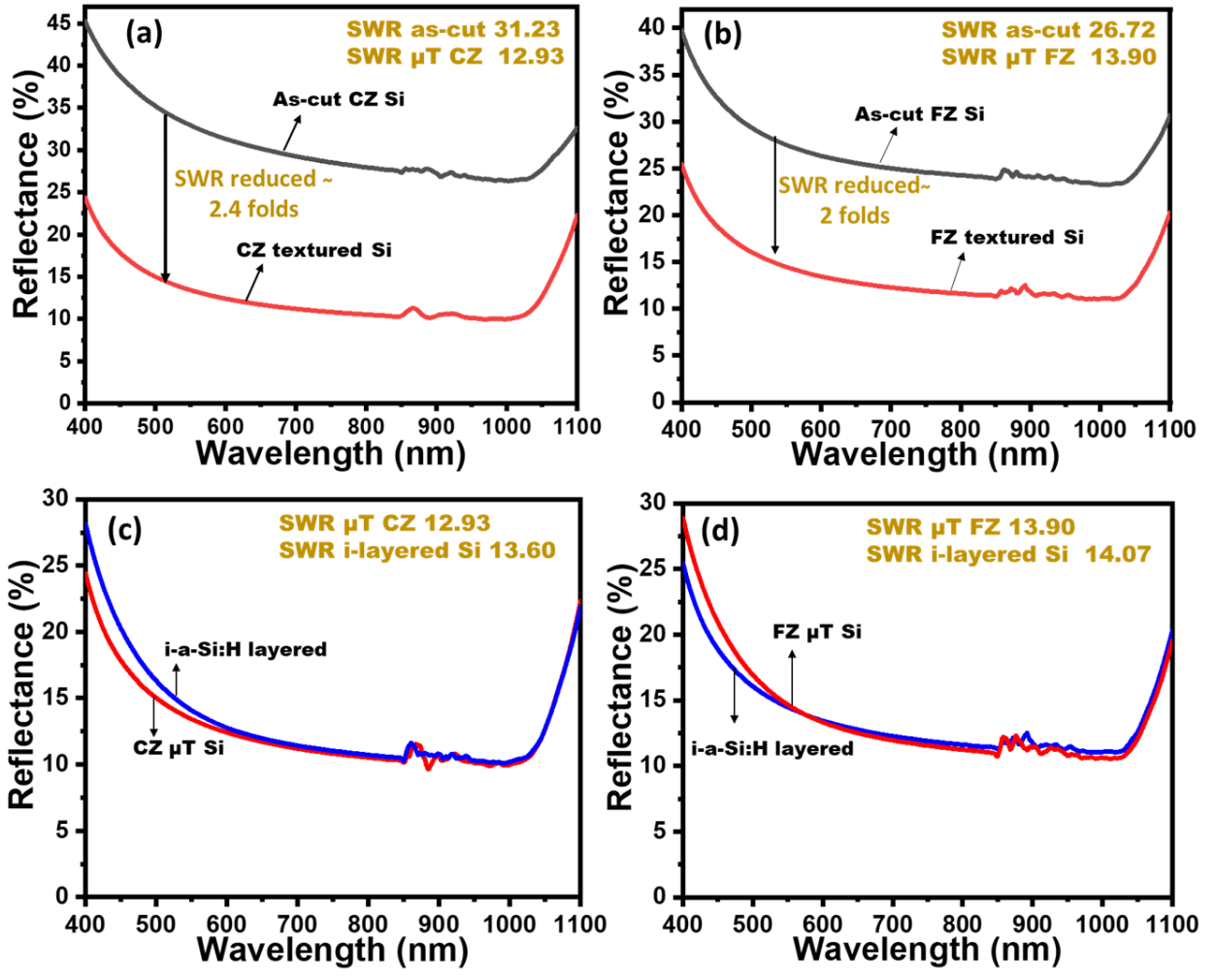

Fig. 3. Comparative diffused optical spectra of (a-b) as-cut and textured CZ-Si and FZ-Si surfaces. (c-d) comparative reflectance spectra before and after i-a-Si:H layer deposition on CZ and FZ Si samples respectively.

3.2. Passivation property of i-a-Si:H and n-nc-Si:H layers on rear side of micro-textured Si surfaces

The surface passivation property (dominating chemical passivation) of the i-a-Si:H layer on the micro-textured CZ and FZ Si rear surfaces was studied and analyzed systematically using the MCLT measurements. The passivation property (dominating field effect passivation) of n-nc-Si:H layer is studied by using concept of induced electric field due to factor like carriers gradient discussed in this section. Both passivation layer together provides effective surface passivation at the rear side of micro-engineered Si surfaces, which is a key-step in fabricating highly efficient either conventional homojunction or modern heterojunction (HIT, Hybrid etc.) solar cells [18]. Importance of surface passivation and details of MCLT measurement of modified Si surfaces for solar cells application have been reported in our earlier work [31]. The dangling bonds (atomic orbital defects) at the Si surfaces being the reason of mid band gap defect or trapped electronic states that act as minority carrier recombination centers which produces non-radiative recombination of the respective carriers [32]. Thus, minimization of such defective electronic states is an important step for effective solar cells fabrication. MCLT experimentally measured by the photo conductance decay method via QSS and transient photo conductance mode using Sinton's instrument (WCT-120). Minority carriers can recombine either in bulk or at the surface defects (shown in Figure 2), therefore an effective recombination rate is measured experimentally. The measured value from each method is the total effective lifetime (τ_{eff}) value that involve the two recombination mechanisms. First is the bulk lifetime (τ_{bulk}) and second is the lifetime of both surfaces of Si (τ_{surf}). It is usually assumed that τ_{bulk} remains unchanged for all the surfaces since no high-temperature processing is carried out [32, 33]. Thus, any change in the τ_{eff} is exclusively due to difference in τ_{surf}, which is directly related to surface defect densities, which effect then the SRV of carries. For a fully passivate surface, τ_{eff} indicate the τ_{surf} due to very high bulk lifetime of carriers. Surface recombination is also quantitatively described in terms of the surface recombination velocity (S_{eff}). The S_{eff} is calculated from the measured value of the τ_{eff}. The limiting value of S_{eff} is calculated using the following expression:

$$\frac{1}{\tau eff} = \frac{1}{\tau bulk} + \frac{1}{\tau surf} \quad (2)$$

Where, $\tau_{surf} = w/2S_{eff}$. Here, S_{eff} is the surface recombination velocity (SRV) and "w" is the wafer thickness (~180µm). The factor "2" is included due to both surfaces contribution. For a fully passivated surface, $\tau_{eff} \cong \tau_{bulk}$, and as $\tau_{bulk} \gg \tau_{surf}$, the τ_{eff} reflects the τ_{surf}. The MCLT measurement was performed on symmetric device structure Figure 4(a).

The i-a-Si:H layer was deposited on each surface of Si materials in order to avoid any effect of upper surface. It was assumed that the quality of the passivated materials also have effect on the passivation capability of the passivation layer and it is demonstrated here experimentally by measuring MCLT for CZ and FZ Si before as well as after deposition of i-a-Si:H layer symmetrically. The observed lifetime for CZ-Si is 2.31 µsec and 677.79 µsec before and after i-a-Si:H layer deposition respectively, similarly 2.77 µsec and 1788.30 µsec before and after i-a-Si:H layer deposition on FZ-Si textured wafers. As can be seen in histogram (Figure 4 (b)), ~ 293.41 folds enhancement in lifetime after incorporating textured CZ-Si surface with intrinsic amorphous layer and ~645.59 folds in case of FZ-Si (Figure 4(c)), proven the excellent passivation behavior of i-a-Si:H layer via chemical passivation (reducing the superficial dangling bond by making suitable bonds with these unfilled electronic states by hydrogen and thus making them H-terminated sites, thus non-reactiveness of defect states and thus passivated the surface) on both type of Si materials [34]. However, influence of material quality on passivation capability of passivation layer can also be seen clearly. As ~ 2.63 fold enhancement in MCLT observed in case of FZ compared to CZ instead both are processed under identical conditions and parameters. This may be attributed to the bulk properties as well as manufacturing process of particular materials i.e. carrier concentration, thickness of wafer, interior defects that related to doping carrier concentration.

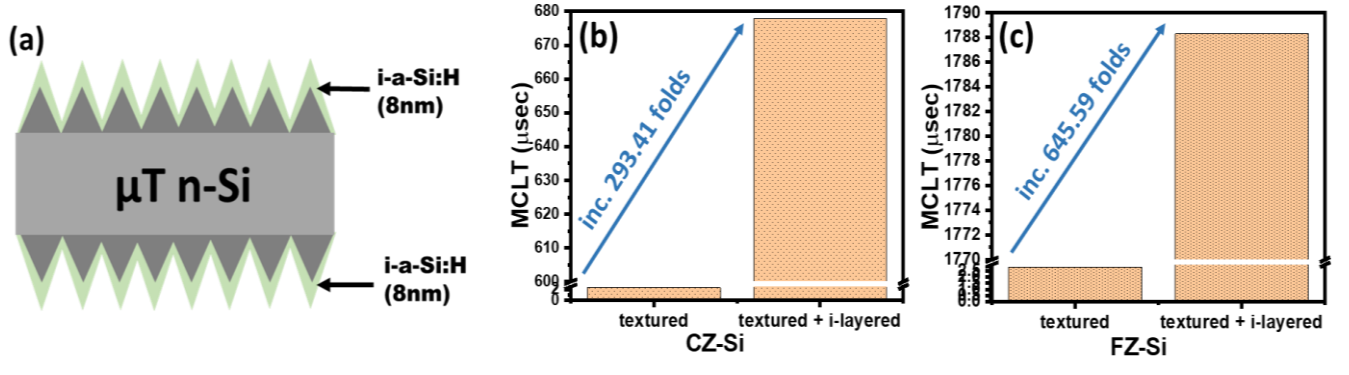

Fig. 4. (a) Symmetric structure for MCLT measurement (i-a-Si:H/µT-n-c-Si/i-a-Si:H), (b) comparison of MCLT of CZ Si samples before and after i-a-Si:H layer deposition and (c) MCLT comparison of FZ textured passivated and unpassivated Si samples respectively.

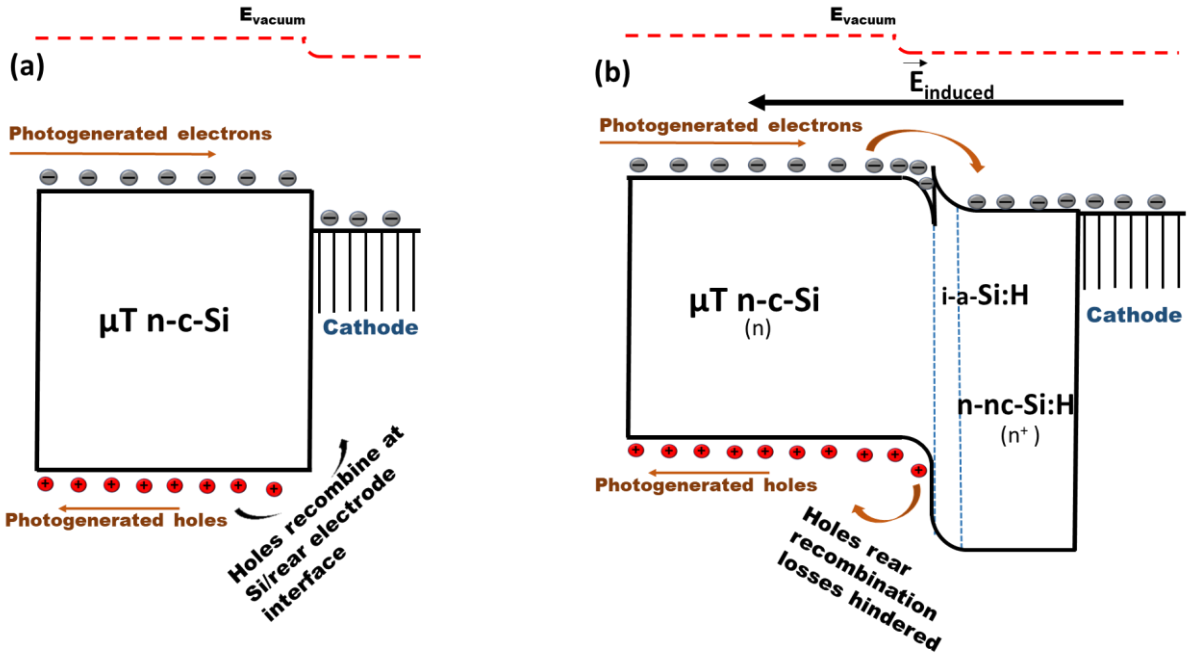

Fig. 5. (a) The band diagram between n-c-Si and rear electrode w/o passivated rear contacts, (b) band diagram of n-c-Si/i-a-Si:H/n-nc-Si:H/rear electrode, clearly showing a high band offset in VB of Si.

Along with passivating the surface, the i-a-Si:H layer act as tunneling layer which provide smooth inter-facial path for carrier transportation and thus reduces parasitic resistance recombination losses up to greater extent which is an another important step in efficient solar cells fabrication [35]. How smoothly carriers transport through this layer depend upon the concentration of hydrogen in i-a-Si layer as well as on thickness of layer itself [36, 37]. Usually amorphous nature of Si is highly absorbing due to non-periodic arrangement of Si atoms, in this arrangement large number of missing states present in the interior geometry of amorphous Si (shown in Figure 2 by green bonds), these states act as trapping states which enhances the absorption via capturing carriers. However, when deposition of i-a-Si layer is performed in presence of hydrogen gas flow these states becomes H-terminated (non-reactive) under controlled parameters (like temperature, silane/hydrogen gas flow rate, power density, frequency) and thus absorbing nature turns into tunneling ones with optimized thickness [27].

The higher passivation quality of i-a-Si:H layer also supported by enhanced implied open circuit voltage (i-V_{oc}) after intrinsic amorphous layer deposition on textured Si wafers. The increment in i-V_{oc} on CZ-Si textured wafer after passivating the surfaces is ~ 1.32 folds, similarly ~ 1.42 folds enhancement for passivated FZ-Si wafers. Thus, the charge carrier collection rate for each material also improved by i-a-Si:H passivation layer. The n-nc-Si:H layer (~ 18 nm) along with i-a-Si:H (~ 8 nm) layer was also deposited at rear side of textured Si wafers to gain effective surface passivation. The n-nc-Si:H layer (53% crystalline) produced from amorphous layer, have tunable optical bandgap that can be tuned to obtained best of it by controlling the crystallinity fraction in amorphous Si taking into consideration other deposition parameters like temperature, silane (SiH_4) gas flow rate, H_2 flow rate, phosphine gas flow rate i.e. doping concentration, power density, pressure, power generating frequency etc [23, 27, 38].

In the present case, n-nc-Si:H layer (have diffused fix charges) is heavily doped (~ 10^{20} cm^{-3}) and n-c-Si (mono crystalline silicon) have a doping carrier density of ~ 10^{15} cm^{-3}, due to carrier concentration gradient (n-n^+), an electric field induced which introduce band bending in-between mono-crystalline and nano crystalline Si surface. This bending of electronic states not only obstruct the photogenerated holes flow towards back electrodes (reduce back surface parasitic recombination losses) but it also accelerates these holes towards anode (front electrode), and make electrons path smoother (via high conductive paths provided by nano crystalline layer by enhance percolation (53% crystalline) in this layer during transformation from amorphous to nano-crystalline geometry). Thus, n-nc-Si:H layer produce back surface field (BSF), which enhance photocarriers transportation towards their respective electrodes and reduces back contact recombination losses. The band alignment is Shown in Figure 5b, indicating a high valance band (VB) offset provided by n-nc-Si:H layer.

However, the intrinsic amorphous layer also provide band offset but in the present case this layer is modulated (via controlling silane /hydrogen gas ratio, very less number of fix charges injected into this layer compared to n-nano-crystalline layer. This will favors dominating chemical passivation nature of amorphous layer) in such a way that its chemical passivating character is dominating one. The n-nc-Si:H layer provide best VB offset, which invert the

photogenerated holes path and reducing the series resistance recombination losses, enhancing the implied open circuit voltages and thus the photogenerated carriers collection rate. The intrinsic amorphous layer provides smooth interface and tunnel carries effectively. Thus, a stack of these layers at rear interface of micro textured Si surfaces provides best back surface passivation which is the most important step in enhancing solar cells efficiency.

4. CONCLUSION

In summary, the simple one-step surface modification alkaline KOH anisotropic process works equivalently on both Si materials and results in enhanced light harvesting property of Si surfaces. The reduced SWR ~ 2.4 folds for CZ-Si compared to as-cut Si and for FZ it decreases ~ 2 folds. However, it is also observed that FZ-Si material needs further optimization for its full potential to harvest light more efficiently. Secondly, rear surface passivation is employed by using stack of i-a-Si:H/n-nc-Si:H layers (8 nm/18 nm), which simultaneously provide effective surface passivation to meet their full potential in reducing back surface recombination/contact losses. The observed MCLT for passivated CZ and FZ Si is 677.79 and 1788.30 µsec respectively compared to unpassivated one which is ~ 2.32 and ~ 2.77 µsec respectively. This clearly indicates the excellent passivation characteristics of the deposited stack of amorphous/nano-crystalline Si thin layers. The i-a-Si:H layer provide enhanced chemical passivation by saturating the dangling bonds of the interface between crystalline and intrinsic amorphous Si. The n-nc-Si:H layer introduce here concept of back surface field, which reduces the parasitic rear recombination losses up to much greater extent. It is observed here that the passivation capability of amorphous layer not only depends upon the deposition parameters, thickness of layer but it depends upon the wafer quality to be passivated (surface morphology as well as bulk material properties). Further, implementation of stack of passivation layer in either HIT, Hybrid or even in conventional solar cells have a great tendency to achieve highly efficient solar cells.

DECLARATIONS

Ethical Approval

Not Applicable

Funding

Not applicable

Availability of data and material

The data of the manuscript are available upon request.

Conflicts of Interest

The authors declare no conflicts of interests. The authors alone are responsible for the content and writing of this article.

Authors' contributions

All the authors contribute equally to the article, in writing and editing

ACKNOWLEDGEMENTS

The authors would like to acknowledge the financial support from the Department of Science and Technology (DST), Government of India, under the Nano Mission, Grant No. DST/NM/NT/ 2023/03(G)/2 (project code: GAP230632) of the Technology Mission Division. The authors are grateful to the Director, CSIR-National Physical Laboratory (NPL), New Delhi, India, for providing research facilities.

REFERENCES

[1] Liu, Y., Li, Y., Wu, Y., Yang, G., Mazzarella, L., Procel-Moya, P., Tamboli, A.C., Weber, K., Boccard, M., Isabella, O. and Yang, X., **2020.** High-efficiency silicon heterojunction solar cells: materials, devices and applications. *Materials Science and Engineering: R: Reports*, *142*, p.100579.

[2] Nishioka, K., Sueto, T. and Saito, N., **2009.** Formation of antireflection nanostructure for silicon solar cells using catalysis of single nano-sized silver particle. *Applied Surface Science*, *255*(23), pp.9504-9507.

[3] Equipment, V.P., **2021**. International technology roadmap for photovoltaic (ITRPV). *Results 2020*, *12*.

[4] Etier, I., Al Tarabsheh, A. and Kannan, N., **2021.** Shunt resistance spatial variations in amorphous silicon solar cells. *Microelectronics Journal*, *108*, p.104960.

[5] Srivastava, S.K., Singh, P., Yameen, M., Prathap, P., Rauthan, C.M.S. and Singh, P.K., **2015.** Antireflective ultra-fast nanoscale texturing for efficient multi-crystalline silicon solar cells. *Solar Energy*, *115*, pp.656-666.

[6] Srivastava, S.K., Kumar, D., Sharma, M., Kumar, R. and Singh, P.K., **2012.** Silver catalyzed nano-texturing of silicon surfaces for solar cell applications. *Solar Energy Materials and Solar Cells*, *100*, pp.33-38.

[7] Srivastava, S.K., Kumar, D., Schmitt, S.W., Sood, K.N., Christiansen, S.H. and Singh, P.K., **2014.** Large area fabrication of vertical silicon nanowire arrays by silver-

assisted single-step chemical etching and their formation kinetics. *Nanotechnology*, *25*(17), p.175601.

[8] Srivastava, A., Sharma, D., Kumari, P., Dutta, M. and Srivastava, S.K., **2021.** Highly efficient PEDOT: PSS/silicon hybrid solar cells via effective surface microengineering of low-cost solar-grade silicon wafers. *ACS Applied Energy Materials*, *4*(4), pp.4181-4198.

[9] Raut, H.K., Ganesh, V.A., Nair, A.S. and Ramakrishna, S., **2011.** Anti-reflective coatings: A critical, in-depth review. *Energy & Environmental Science*, *4*(10), pp.3779-3804.

[10] Singh, P., Srivastava, S.K., Sivaiah, B., Prathap, P. and Rauthan, C.M.S., **2018.** Enhanced photovoltaic performance of PEDOT: PSS/Si solar cells using hierarchical light trapping scheme. *Solar Energy*, *170*, pp.221-233.

[11] Yao, C., Liu, Y., Niu, J., Lu, C., Li, H. and Xie, C., **2024.** Micro/nano-hybrid hierarchical structure of black silicon decorated with gold nanoparticles for ultralow broadband reflectivity (< 1%). *Applied Surface Science*, *655*, p.159641.

[12] Singh, P.K., Kumar, R., Lal, M., Singh, S.N. and Das, B.K., **2001.** Effectiveness of anisotropic etching of silicon in aqueous alkaline solutions. *Solar Energy Materials and Solar Cells*, *70*(1), pp.103-113.

[13] Seidel, H., Csepregi, L., Heuberger, A. and Baumgärtel, H., **1990.** Anisotropic etching of crystalline silicon in alkaline solutions: I. Orientation dependence and behavior of passivation layers. *Journal of the electrochemical society*, *137*(11), p.3612.

[14] Seidel, H., **1990.** Orientation Dependence and Behaviar of Passivation Layers. *J. Electrochem. Soc.*, *137*, p.3626.

[15] Giles, F.P., Schwartz, R.J. and Gray, J.L., **1993,** May. Interpretation of microwave-detected photoconductance decay lifetime measurements. In *Conference Record of the Twenty Third IEEE Photovoltaic Specialists Conference-1993 (Cat. No. 93CH3283-9)* (pp. 299-302). IEEE.

[16] Srivastava, A., Sharma, D. and Srivastava, S.K., **2023.** Impedance spectroscopy analysis to probe the role of interface properties of surface micro-engineered PEDOT: PSS/n-Si solar cells. *Organic Electronics*, *119*, p.106817.

[17] Sinton, R.A., Cuevas, A. and Stuckings, M., **1996,** May. Quasi-steady-state photoconductance, a new method for solar cell material and device characterization. In *Conference Record of the Twenty Fifth IEEE Photovoltaic Specialists Conference-1996* (pp. 457-460). IEEE.

[18] Bonilla, R.S. and Wilshaw, P.R., **2013.** Stable field effect surface passivation of n-type Cz silicon. *Energy Procedia*, *38*, pp.816-822.

[19] Kerr, M.J. and Cuevas, A., **2001.** Very low bulk and surface recombination in oxidized silicon wafers. *Semiconductor science and technology*, *17*(1), p.35.

[20] He, J., Ling, Z., Gao, P. and Ye, J., **2017.** TiO_2 Films from the Low-Temperature Oxidation of Ti as Passivating-Contact Layers for Si Heterojunction Solar Cells. *Solar RRL*, *1*(12), p.1700154.

[21] Kumari, P., Punia, U., Sharma, D., Srivastava, A. and Srivastava, S.K., **2023.** Enhanced photovoltaic performance of PEDOT: PSS/Si heterojunction Solar cell with ZnO BSF layer: a simulation study using SCAPS-1D. *Silicon*, *15*(5), pp.2099-2112.

[22] Yang, X., Bi, Q., Ali, H., Davis, K., Schoenfeld, W.V. and Weber, K., **2016.** High-Performance TiO2-Based Electron-Selective Contacts for Crystalline Silicon Solar Cells. *Advanced Materials (Deerfield Beach, Fla.)*, *28*(28), pp.5891-5897.

[23] Yang, X., Zheng, P., Bi, Q. and Weber, K., **2016.** Silicon heterojunction solar cells with electron selective TiOx contact. *Solar Energy Materials and Solar Cells*, *150*, pp.32-38.

[24] Page, M.R., Iwaniczko, E., Xu, Y.Q., Roybal, L., Hasoon, F., Wang, Q. and Crandall, R.S., **2011.** Amorphous/crystalline silicon heterojunction solar cells with varying i-layer thickness. *Thin Solid Films*, *519*(14), pp.4527-4530.

[25] Agarwal, M., Pawar, A., Wadibhasme, N. and Dusane, R., **2017.** Controlling the c-Si/a-Si: H interface in silicon heterojunction solar cells fabricated by HWCVD. *Solar Energy*, *144*, pp.417-423.

[26] Etier, I., Al Tarabsheh, A. and Kannan, N., **2021.** Shunt resistance spatial variations in amorphous silicon solar cells. *Microelectronics Journal*, *108*, p.104960.

[27] Bhattacharya, S., Pandey, A., Alam, S. and Komarala, V.K., **2024.** Development of high conducting phosphorous doped nanocrystalline thin silicon films for silicon heterojunction solar cells application. *Nanotechnology*, *35*(32), p.325701.

[28] Cho, W.J., Chin, W.K. and Kuo, C.T., **2004.** Effects of alcoholic moderators on anisotropic etching of silicon in aqueous potassium hydroxide solutions. *Sensors and Actuators A: Physical*, *116*(2), pp.357-368.

[29] Sharma, D., Srivastava, A., Tawale, J.S., Prathap, P. and Srivastava, S.K., **2023.** High efficiency flexible PEDOT: PSS/silicon hybrid heterojunction solar cells by

employing simple chemical approaches. *Journal of Materials Chemistry C*, *11*(39), pp.13488-13502.

[30] National Renewable Energy Laboratory (NREL) (https://www.nrel.gov/solar)

[31] Batra, N., Kumar, S., Sharma, M., Srivastava, S.K., Sharma, P. and Singh, P.K., **2012.** A comparative study of silicon surface passivation using ethanolic iodine and bromine solutions. *Solar energy materials and solar cells*, *100*, pp.43-47.

[32] Schroder, D.K., **1997.** Carrier lifetimes in silicon. *IEEE transactions on Electron Devices*, *44*(1), pp.160-170.

[33] Schenk, A., **1992.** A model for the field and temperature dependence of Shockley-Read-Hall lifetimes in silicon. *Solid-State Electronics*, *35*(11), pp.1585-1596.

[34] Pandey, A., Bhattacharya, S., Panigrahi, J., Mandal, S. and Komarala, V.K., **2023.** Investigation of dual intrinsic a-Si: H films for crystalline silicon surface passivation by spectroscopic ellipsometry: application in silicon heterojunction solar cells. *Applied Physics A*, *129*(8), p.575.

[35] Kanevce, A. and Metzger, W.K., **2009**. The role of amorphous silicon and tunneling in heterojunction with intrinsic thin layer (HIT) solar cells. *Journal of Applied Physics*, *105*(9).

[36] Pandey, A., Bhattacharya, S., Panigrahi, J., Mandal, S. and Komarala, V.K., **2022.** Effect of gas flow rate in PECVD of amorphous silicon thin films for interface passivation of silicon heterojunction solar cells. *physica status solidi (a)*, *219*(16), p.2200183.

[37] Mikolášek, M., Nemec, M., Vojs, M., Jakabovič, J., Řeháček, V., Zhang, D., Zeman, M. and Harmatha, L., **2014.** Electrical transport mechanisms in amorphous/crystalline silicon heterojunction: Impact of passivation layer thickness. *Thin Solid Films*, *558*, pp.315-319.

[38] Yan, B., Yue, G., Yang, J. and Guha, S., **2013.** On the bandgap of hydrogenated nanocrystalline silicon intrinsic materials used in thin film silicon solar cells. *Solar Energy Materials and Solar Cells*, *111*, pp.90-96.